Paleoclimate in continental northwestern Europe during the Eemian and early Weichselian (125-97 ka): insights from a Belgian speleothem.

Stef Vansteenberge[1], Sophie Verheyden[1,2], Hai Cheng[3,4], R. Lawrence Edwards[4], Eddy Keppens[1] and Philippe Claeys[1]

Correspondence to: S. Vansteenberge (svsteenb@vub.ac.be)

[1]Earth System Science Group, Analytical-, Environmental- & Geo-Chemistry, Vrije Universiteit Brussel, Brussels, Belgium
[2]Royal Belgian Institute for Natural Sciences, Brussels, Belgium
[3]Institute of Global Environmental Change, Xi'an Jiaotong University, Xi'an, China
[4]Department of Earth Sciences, University of Minnesota, Minneapolis, USA

Abstract. The last interglacial serves as an excellent time interval for studying climate dynamics during past warm periods. Speleothems have been successfully used for reconstructing the paleoclimate of last interglacial continental Europe. However, all previously investigated speleothems are restricted to southern Europe or the Alps, leaving large parts of northwestern Europe undocumented. To better understand regional climate changes over the past, a larger spatial coverage of European last interglacial continental records is essential and speleothems, because of their ability to obtain excellent chronologies, can provide a major contribution. Here, we present new, high-resolution data from a stalagmite (Han-9) obtained from the Han-sur-Lesse Cave in Belgium. Han-9 formed between 125.3 and ~97 ka, with interruptions of growth occurring at 117.3 – 112.9 ka and 106.6- 103.6 ka. The speleothem was investigated for its growth, morphology and stable isotope (δ^{13}C and δ^{18}O) composition. The speleothem started growing relatively late within the last interglacial, at 125.3 ka, as other European continental archives suggest that Eemian optimum conditions were already present during that time. It appears that the initiation of Han-9 growth is caused by an increase in moisture availability, linked to wetter conditions around 125.3 ka. The δ^{13}C and δ^{18}O proxies indicate a period of relatively stable conditions after 125.3 ka, however, at 120 ka the speleothem δ^{18}O registered the first signs of regionally changing climate conditions, being a modification of ocean source δ^{18}O linked to an increase in ice volume towards the Marine Isotope Stage (MIS) 5e-5d transition. At 117.5 ka, drastic vegetation changes are recorded by Han-9 δ^{13}C immediately followed by a cessation of speleothem growth at 117.3 ka, suggesting a transition to significantly dryer conditions. The Han-9 record covering the early Weichselian displays larger amplitudes in both isotope proxies and changes in stalagmite morphology, evidencing increased variability compared to the Eemian. Stadials that appear to be analogous to those in Greenland are recognized in Han-9 and the chronology is consistent with other European (speleothem) records. Greenland Stadial 25 is reflected as a cold/dry period within Han-9 stable isotope proxies and the second interruption in speleothem growth occurs simultaneously with Greenland Stadial 24.

Keywords. paleoclimate, last interglacial, Eemian, northwestern Europe, speleothem, stable isotopes, millennial-scale variability, Greenland stadials

1 Introduction

The last interglacial (LIG) period is known as the time interval before the last glacial period during which temperatures were similar to or higher than those of the Holocene period and Present Day (Otto-Bliesner et al., 2013). In marine sediment cores, the LIG is defined as Marine Isotope Stage (MIS) 5e (Shackleton, 1969). The start and end of the MIS 5e period are conventionally set at 130 and 116 ka, respectively, based on marine records (e.g. Martinson et al., 1987). The expression of the LIG in continental western Europe is defined as the Eemian, although it does not coincide precisely with the isotopically constrained MIS 5e (Otvos, 2015). Given the ongoing debate about the LIG nomenclature, clarification about the terms used in this manuscript is required. This study focusses on speleothem archives, thus the terms "Eemian" and "Weichselian" are preferred in the context of European continental paleoclimate. The Eemian is defined as the optimum or acme LIG climate conditions (the "sensu stricto" definition). Subsequent to the Eemian, the Weichselian starts, with the early Weichselian in continental records corresponding to the time-equivalent of MIS 5d – 5a. "Glacial inception" is considered to be informal and only marks the Eemian to early Weichselian transition.

The term "Eemian" was originally introduced by P. Harting in1875 and was characterized by the occurrence of warm water mollusks in marine sediments of the Eem River valley, near Amsterdam, the Netherlands. Nowadays, the Eemian is mostly interpreted as an interval of warmer climate associated with the spread of temperate mixed forests in areas with similar vegetation to today (Kukla et al., 2002). However, the Eemian is also known to be a diachronous unit (Kukla et al., 2002; Wohlfarth et al. 2013), with a longer duration of up to 20 ka, from 130 to 110 ka, in southern Europe as evidenced by pollen records (Sanchez Goñi et al., 1999; Tzedakis et al., 2003). The LIG period exhibited global mean temperatures (GMT) 1.5° to 2°C higher than the pre-anthropogenic average together with peak eustatic sea levels that were between 5.5 and 9m higher than present (Dutton and Lambeck, 2012). Therefore, the LIG gained a lot of attention from both paleoclimate and climate modelling communities for studying a warmer climate state and potential future sea-level rise (Loutre et al., 2014; Goelzer et al., 2015), even though the present-day configuration of Earth's orbital forcing parameters is different (Berger and Loutre, 2002). Following the Eemian, climate went into a glacial mode known as the last glacial cycle, or the Weichselian in the western European continental terminology, which lasted until the Holocene. A major feature of climate variability during the last glacial is the occurrence of millennial-scale, rapid cold-warm-cold cycles, known as Dansgaard-Oeschger (D/O) events (Bond et al., 1993). These D/O cycles are expressed as alternating Greenland stadial (GS) and interstadial (GIS) phases in Greenland ice cores (Dansgaard et al., 1993; NGRIP members, 2004) and they also have affinity with Atlantic cold events registered in sea-surface temperature proxies (McManus et al., 1994). Some of the stadials are also associated with an increased flux of ice rafted debris (IRD) in the North Atlantic Ocean (McManus et al., 1994). These events have been linked to changes in the strength and shifts in the northwards extent of Atlantic Meridional Overturning Circulation (AMOC) (Broecker et al., 1985). The exact cause of such changes in the AMOC mode is still debated. Nevertheless, according to Barker et al. (2015), it is more likely a non-linear response of a gradual cooling of the climate than a result of enhanced fresh-water input by iceberg calving, as previously proposed by Bond et al. (1995) and van Kreveld et al. (2000). Likewise, continental pollen records extracted from cores of Eifel Maar lakes (Sirocko et al., 2005) or peat bogs in the Vosges, France (Woillard, 1978; de Beaulieu and Reille, 1992; de Beaulieu, 2010), have recorded changes in pollen assembly, attributed to D/O variability. So far, up to 26 GS's have been identified in ice-cores, with GS 26 recognized as corresponding to the end of the Eemian interglacial period (NGRIP members, 2004).

Speleothems are ideal for late Quaternary paleoclimate studies because of their ability to obtain accurate chronologies with U/Th dating of up to 600 ka and their potential to yield high resolution (up to seasonal scale) paleoclimate records (Fairchild and Baker, 2012). The speleothem records covering the Eemian and early Weichselian in Europe have provided detailed paleoclimate reconstructions (Genty et al., 2013). Several speleothem stable isotope proxies from Europe record optimum climatic conditions during the Eemian (Meyer et al., 2008; Couchoud et al., 2009) and D/O climate events during the early Weichselian (Bar-Matthews et al., 1999; Drysdale et al., 2007; Boch et al. 2011). Yet so far, all records covering that time period are located in southern Europe (Italy, southern France, Levant) or the Alps. This study presents a new high-resolution speleothem dataset from Belgium that expands the European coverage of last interglacial speleothem archives northwards.

Earlier chronostratigraphic work on speleothem deposits and detrital sediments within Belgian caves marked the presence of glacial/interglacial cycles, with speleothem formation restricted to interglacial periods, when warm and wet climates favored growth. Detrital sediments settle in colder periods, with river deposits in cold wet periods and reworked loams during cold dry periods (Quinif, 2006). From the 1980's onwards, speleothems covering MIS 9 to 1 have been found in various Belgian caves (Bastin and Gewelt, 1986; Gewelt and Ek, 1988). Quinif and Bastin (1994) analyzed an Eemian flowstone from the Han-sur-Lesse Cave for its pollen composition, and demonstrated that vegetation above the cave area reflects interglacial climate optimum conditions around 130 +/- 10 ka. However, the dating of this material contains large uncertainties related to the alphaspectrometric methodology used. This study focusses on a recently obtained speleothem, Han-9 from the Han-sur-Lesse Cave in southern Belgium. This stalagmite was analyzed to better constrain 1) the chronology of Eemian optimum conditions in Belgium and 2) the occurrence and signature of millennial-scale climate variability (D/O) over northwestern Europe during the early Weichselian.

2 Han-sur-Lesse Cave: geology and cave parameters

The Han-sur-Lesse Cave system is the largest known subterranean karst network in Belgium, with a total length of ~10km. It is located within the *Calestienne*, a SW-NE trending superficial limestone belt of Middle Devonian age. After deposition, these Paleozoic sediments underwent Hercynian folding followed by Mesozoic erosion. The current hydrographic network was established during the Neogene and Pleistocene, by erosion into these folded belts (Quinif, 2006). The cave system was formed within the *Massif du Boine*, part of an anticline structure consisting out of Middle to Late Givetian reefal limestones, by a meander shortcut of the Lesse River (Fig. 1B). The thickness of the epikarst zone above the cave is estimated to be around 40m.

The area of the Han-sur-Lesse Cave is located ~200km inland at an elevation of 200m above sea level (Fig. 1) and is marked by a maritime climate with cool summers and mild winters. For the period 1999-2013, average year-temperature above the cave was 10.2°C and average yearly rainfall amount 820mm yr^{-1}. The amount of precipitation does not follow a seasonal distribution (Royal Meteorological Institute, RMI). The dominant moisture source in northwestern Europe is the North Atlantic Ocean, and this remains constant throughout the year (Gimeno, 2010). Modern $\delta^{18}O$ of rainfall seasonally varies between -17‰ in winter and -4‰ in summer (Van Rampelbergh et al., 2014). The area above the cave mainly consists of C3 type vegetation with *Corylus*, *Fagus* and *Quercus* trees, and as a natural reserve it has been protected from direct human influence for over 50 years (Timperman, 1989). The Lesse River enters the cave system at the *Gouffre de Belveaux* and exits at the *Trou de Han* approximately 24 hours later. The Han-9 stalagmite was collected within the *Réseau Renversé*, which is the most distal part of the *Réseau Sud* (Fig. 1B). The natural connection between the *Réseau Sud* and

other parts of the Han-sur-Lesse Cave is fully submerged, but in 1960 an artificial tunnel was established facilitating access (Timperman, 1989). When water of the Lesse River is high, part of the stream is redirected through the *Réseau Sud* but it does not reach the *Réseau Renversé* (Bonniver, 2010). Earlier studies have shown that cave drip waters are mostly supplied by diffuse flow through the host rock (Bonniver et al., 2011; Van Rampelbergh et al., 2014). The Han-sur-Lesse Cave is partly accessible for tourists, but because of the difficult access, the *Réseau Sud* is protected from any anthropogenic influence. Temperature logging for six months with an interval of two hours in the *Réseau Renversé* shows an average cave temperature of 9.45°C with a standard deviation < 0.02°C, which reflects the average temperature of 9.2°C above the cave for 2013. Minimum and maximum temperatures were 9.39°C and 9.51°C, respectively (C. Burlet, pers. comm.). This shows that the temperature in the *Réseau Renversé* is constant through the year and that it reflects the average temperature above the cave. In contrast, recent cave monitoring in more ventilated parts of the cave indicated a temperature seasonality of 3°C (Van Rampelbergh et al., 2014). For the *Réseau Renverse*, there are no indications that cave morphology changed significantly since the last interglacial. Han-9, the stalagmite presented in this study, was deliberately sampled because it was already broken into three parts, so no other speleothems had to be destroyed. Although the sample was broken, it was still in situ. The candle-shaped stalagmite has a length of 70cm (Fig. 2C-E).

The Han-sur-Lesse Cave received scientific attention in the last decades, making it the best understood cave system in Belgium. This includes detailed hydrographic studies (Bonniver et al., 2010) and extended cave monitoring surveys (Verheyden et al., 2008; Van Rampelbergh et al., 2014), leading to successful paleoclimate reconstructions on Holocene speleothems down to seasonal scale (Verheyden et al., 2006; 2012; 2014; Van Rampelbergh et al., 2015). The elaborate cave monitoring (Fig. 1B) has provided a solid foundation for understanding the cave system and to interpret its paleoclimate records, even back to ~120 ka.

3 Methods and analytical procedures

All ages were acquired by using U/Th dating at the University of Minnesota Earth Sciences Department, Minneapolis. Nine samples were analyzed in 2013 and an additional batch of 14 samples was dated in 2015 to further improve the age-depth model with additional sampling locations selected based on the preliminary age model and the stable isotope (δ^{13}C and δ^{18}O) data (Fig. 2D). For all U/Th analyses, 150-200mg of speleothem calcite was milled and analyzed with a Neptune multiple-collector plasma source mass spectrometer (MC-ICP-MS) from Thermo-Scientific. Ages were corrected assuming an initial ^{230}Th/^{232}Th atomic ratio of 4.4 ±2.2 x 10^{-6}. The age datum is 1950 CE. For additional information about the applied method, see Edwards et al. (1987), Shen et al. (2012) and Cheng et al. (2013) and references therein. Age-depth modeling was carried out using the StalAge algorithm of Scholz and Hoffmann (2011). All depths are expressed in 'mm dft' with dft being 'distance from top'.

All stable isotope analysis were carried out at the Stable Isotope Laboratory, Vrije Universiteit Brussel. A total of 1118 samples were drilled with a Merchantek MicroMill, a computer steered drill mounted on a microscope. Samples were taken along the central growth axis to avoid possible effects of evaporation during calcite deposition (Fairchild et al., 2006). For all samples, tungsten carbide dental drill bits with a diameter of 300µm from Komet were used. As a function of the growth rate, 1000, 500 and 250µm sampling resolutions were applied in order to maintain a more or less equal resolution in the time domain. For sample locations, see Fig. 2D. Samples were kept at 50°C prior to analysis to avoid contamination. δ^{13}C and δ^{18}O isotope measurements were performed on a Perspective IRMS from Nu Instruments, coupled to a Nucarb automated carbonate

preparation system and a minor amount (<100) on a Kiel III device coupled to a Delta plus XL from Thermo-Scientific. Two samples of the in-house standard MAR-2(2), made from Marbella limestone and which has been calibrated against the international standard NBS-19 (Friedman et al., 1982), were measured every 10 samples to correct for instrumental drift. Reported values for the MAR-2(2) are 0.13‰ Vienna Pee Dee Belemnite (VPDB) for δ^{18}O and 3.41‰ VPDB for δ^{13}C. Analytical uncertainties on standards from individual batches were $\leq$ 0.05‰ for δ^{13}C and $\leq$ 0.08‰ for δ^{18}O on the Nu Instruments setup. At regular intervals, a replicate sample was measured in a different batch to check for the reproducibility of the analytical method. Outliers were manually detected, removed and re-measured if sufficient material was present. In addition, six 30μm thin-sections were taken along the growth transect (Fig. 2D).

4 Results

4.1 Speleothem morphology

Figures 2C-2E show the interpretation of the internal morphology of Han-9. In the lower part of the speleothem, below 365mm dft, the calcite was well-laminated alternating between thick white and slightly darker layers. In the lower 15mm, some fine, brown detrital laminae can be seen, although they are confined to the very base and the lateral sides of the stalagmite. From 430mm dft, the calcite becomes progressively coarser and layering less expressed with alternations between thicker parts of denser and coarser calcite. Starting from 365mm dft, the speleothem calcite has a very coarse appearance and layering is almost indistinguishable. This goes on until 304mm dft, where a first discontinuity in growth, D1, appears. This discontinuity was identified macroscopically. After D1, 100mm of speleothem is characterized by alternating bands of dense and dark brown calcite with coarser, white calcite. Between 200 and 176mm dft, a band of dense, brown calcite is present. Within this band, very fine laminae of red-brown material can be observed. This band ends with a second discontinuity, D2. Following D2, the axis of growth for the next 20mm is tilted to the right. The entire upper section consists of dense and dark brown calcite, with little variation except for a coarser interval between 58 and 40mm dft. Besides some subtle unconformities marked by the dashed lines in Fig. 2D, no internal layering is visible macroscopically. Thin-section locations were chosen as representative of the typical morphologies displayed in the stratigraphic log in Fig. 2E. Fabrics are described according to Frisia (2015). In all thin sections, the dominant fabric of the calcite crystals was columnar (Fig. 3A). The layering, although often very well displayed macroscopically, was not distinguishable within the thin sections. Variations in fabric occur between macroscopically defined 'denser' and 'coarser' calcite (Fig. 2E), where the latter has smaller columnar calcite crystals with significantly more inter-crystalline porosity often filled with fluid inclusions (Fig. 3B), and thereby described as columnar open. The denser morphology has substantially larger crystals with almost no pore space and can be defined as columnar elongated. Another type of fabric occurs within the dark brown band of dense calcite between 200 and 176mm dft. There, the columnar fabric is replaced with smaller more equant calcite crystals (Fig. 3C), which are then followed by a fine layer of brown detrital material representing D2.

4.2 U/Th dating

The results of U/Th dating are shown in Table 1. Dating samples are labeled by "DAT-X", with X representing the sample number in Fig. 2D. All ages are displayed as "ka". In all samples, the detrital Th content, estimated by ^{232}Th concentration and the initial ^{230}Th/^{232}Th atomic ratio, is relatively low (range: 6419 – 208 ppt). This leads to only minor corrections for the ^{230}Th age (Table 1). Errors are given as 2σ and range between ±212 years and ±666 years. The U and Th concentrations determined in the 2013 samples allowed reduction of the sample

size, resulting in smaller errors for the 2015 samples. From 672 to 176mm dft, all ages are stratigraphically consistent; no age inversions occur when taking into account the 2σ error of the U/Th ages. Between 176 and 0mm dft, the distribution of the ages is more chaotic, with the occurrence of several age inversions and outliers.

4.3 Stable isotopes: δ^{13}C and δ^{18}O

Figures 2A and B show the results of the δ^{13}C and δ^{18}O analyses, plotted against sample depth in mm dft. All values are expressed in ‰ VPDB. The δ^{13}C varies between -3.58 and -10.30‰, with an average of -7.53‰. The δ^{18}O values show smaller variations, between -5.04 and -7.02‰, with an average of -5.91‰. Lower amplitude variability in both δ^{13}C and δ^{18}O occur in the lower part of the stalagmite, and larger amplitude variations are present from ~400mm dft upwards, corresponding to distinct transitions in morphology (alternating zones of dense, more brown and coarser, more white calcite, Fig. 2E).

5 Discussion

5.1 Age model

The StalAge algorithm (Scholz and Hoffmann, 2011) was applied to the individual ages in order to construct an age-depth model, displayed in Fig. 4. It is clear that the stalagmite endured three separate growth phases, and that the discontinuities, expressed in the stalagmite morphology at 302 and 176mm dft (Fig. 2D), correspond to two hiatuses separating these three growth phases. In the first growth phase, all ages are in stratigraphic order and are included within the model and the 2σ error. DAT-1 has only limited weight in the final model and an explanation for this is given in the algorithm specifications (Scholz and Hoffmann, 2011). During the modeling process, the StalAge algorithm has a step where the data is screened for the occurrence of minor outliers and age inversions. This is done by fitting error weighted straight lines through subsets of three adjacent data points. However, DAT-1 is located in the basal part of the stalagmite, so less subsets of three data points can be used including DAT-1. If DAT-1 does not fit on the error weighted straight line created with the adjacent data points DAT-10 and DAT-11, which is the case here, the error of DAT-1 will be increased and the weight of DAT-1 in the Monte Carlo simulation for the age fitting will decrease. This results in less solutions where DAT-1 is included in the Monte Carlo simulated age models. The occurrence of substantial changes in growth rate in the boundary areas of a speleothem sample is recognized as a limitation of the StalAge algorithm (Scholz and Hoffmann, 2011). Even though the three growth phases were modeled separately with StalAge, the model does not perform well with the start of the Hiatus 2, as DAT-19 is completely excluded. Likely, this is again caused by the fact that DAT-19 is located in a boundary area. Here, the stalagmite petrography shows clear evidence of a significantly decreased growth rate after DAT-16 (110.6 ka), i.e. very dense, brownish calcite with fine laminae (Fig. 2C and E). In complex cases, such as in this study where multiple hiatuses occur, the simplest model is still the best. Therefore, linear interpolation combined with good observations of changes in petrography, was applied to include DAT-19 within the age model (Fig. 4, red line). For the third growth phase, because of the occurrence of several age inversions, the resulting age model is unreliable. Despite the fact that ages clearly cluster between ~103 and ~97 ka, the chronology of the third growth phase is only poorly constrained and therefore a detailed interpretation of Han-9 in terms of paleoclimate is limited to the first two growth phases.

The first growth phase starts at 125.34 +0.78/-0.66 ka with stable growth-rate of 0.02mm yr^{-1} up to around 120.5 ka. After that, the growth rate significantly increases, with values up to 0.15mm yr^{-1}. At 117.27 +0.69/-1.02 ka, growth ceases and the first hiatus, H1, starts. The hiatus lasts 4.41 +1.10/-1.49 ka and at 112.86 +0.47/-0.41 ka growth phase 2 starts. DAT-4 and DAT-5 were taken 6mm below and above the discontinuity and the age-depth model does not show any reason to question the timing of H1. As for the second growth phase, growth-rate remains at a constant pace of 0.04mm yr^{-1} until approximately 110.5 ka, where it decreases to 0.006mm yr^{-1}. At 106.59 +0.21/-0.22 ka, the second growth phase ends. Given this age-depth model, stable isotopes were analyzed with a temporal resolution between 100 and 0.3 years, and an average of 16 years.

5.2 Interpretation of stable isotope proxies

5.2.1 Isotopes deposited in isotopic equilibrium?

The best test for the presence of kinetic fractionation is to have a reproducible record (Dorale and Liu, 2009). However, in the absence of a second stalagmite record, Hendy tests could be performed (Hendy, 1971). The problem here is that growth rates are rather low and the layering very fine, so it would be hard to sample precisely in one layer. Therefore, an additional test for correlation of δ^{13}C and δ^{18}O was done by calculating the Pearson's correlation coefficient on the entire record and on the three growth phases separately (Table 2). Yet, a correlation between δ^{13}C and δ^{18}O does not give conclusive evidence for the presence of kinetic fractionation, as both δ^{13}C and δ^{18}O are expected to be controlled by climate and could therefore show positive or negative covariation (Dorale and Liu, 2009). The Pearson's coefficients reveal that there is a clear difference between the separate growth phases. The first growth phase, with $\rho = 0.024$, marks no covariation. The second growth phase, with $\rho = -0.467$, has a substantial degree of negative covariation, whereas the third growth phase ($\rho = 0.461$) has a positive covariation. The differences between the coefficients of the separate growth phases indicate that several processes are controlling the stable isotope variability and that the presence or absence of covariation reflects changes in climate conditions between the growth phases rather than the presence or absence of equilibrium. Nevertheless, equilibrium deposition between the drip water and recent calcite in Han-sur-Lesse Cave has been observed by Van Rampelbergh et al. (2014).

5.2.2 Variations in speleothem δ^{13}C

The δ^{13}C in Han-9 is controlled by changes in vegetation assembly above the cave. This is deduced from the match between Han-9 δ^{13}C and the abundance of grass pollen in the assembly of Sirocko et al. (2005) recovered from the Eifel maar (Fig. 1A and Fig. 5). The agreement between Han-9 δ^{13}C and the Eifel pollen assembly is remarkable; increases in δ^{13}C occur when the percentage of grass pollen increases in the Eifel record. Similar shifts in grass/forest vegetation have even been observed the Vosges region, France, 300km further south (Woillard, 1978; de Beaulieu and Reille, 1992; de Beaulieu, 2010) and in other records from northern and central Europe (Helmens, 2014 and references therein). Also, the δ^{13}C of recent calcite formed with a current forest-type vegetation above the cave is ~-8‰ (Table 3). These values are similar to those observed during the last interglacial in Han-9 (125.3-117.3 ka, Fig. 5). Changes in δ^{13}C of several per mil are often attributed to changes in C3 versus C4 plants (McDermott, 2004). However, a higher abundance of grasses does not necessarily result in an increased amount of C4 vegetation. First of all, C4 species only make up ~1% of the total amount of vascular plant species in northwestern Europe today (Pyankov et al., 2010). Secondly, C4 species dominantly occur in a warmer, tropical climate (Ehleringer et al., 1997). Finally, within the subfamily of the Poideae, commonly referred to as the cool-season grasses and thriving in temperate European climate, all species use the

C3 pathway (Soreng et al., 2015). The reason why speleothem calcite tends to be enriched in ^{13}C when vegetation is dominated by grasses is because grasses have a smaller biomass than trees and also the amount of soil respiration is lower, both leading to a smaller fraction of biogenic CO_2 compared to (heavier) atmospheric CO_2 within the soil (Genty et al., 2003). The similarity between the two records does not seem to hold up after 109 ka. From here on, δ^{13}C becomes more depleted while the Eifel record shifts towards an assembly dominated by grasses. It is not clear what might have caused this depletion, but since growth rates are very low after 109 ka (Fig. 4), it could be related to prior calcite precipitation (PCP). PCP is known to act as a control mechanism on seasonal variations in δ^{13}C of Han-sur-Lesse speleothems, as concluded from an elaborate cave monitoring study by Van Rampelbergh et al. (2014). However, the study by Van Rampelbergh et al. (2014) was carried out on a large, tabular-shaped stalagmite with drip water discharge rates of 300mL min-1 and growth rates of ~1mm yr-1, so caution is required when extrapolating these cave monitoring conclusions to smaller, slower growing stalagmites in a different part of the cave system. If PCP occurs at one site in the cave, it does not mean that it occurs over the entire cave (Riechelmann et al., 2011). Since no additional data on Sr and Mg is currently available for Han-9, the presence of PCP cannot be confirmed, neither rejected.

To summarize, the control on Han-9 δ^{13}C variations is the amount of biogenic CO_2 in the soil, caused by changes in the vegetation type above the cave (forest/grasses) which is directly linked to climate. Lower, depleted δ^{13}C values occur during warmer and wetter periods, when vegetation is dominated by temperate trees. Higher, enriched δ^{13}C values of speleothem calcite correspond with a higher abundance of grasses above the cave during colder/dryer climate intervals.

5.2.3 δ^{18}O

In mid-latitude Europe, several different processes (including temperature, amount effect and ocean source) influence speleothem δ^{18}O variability (McDermott, 2004). A good overview of all processes possibly influencing the speleothem δ^{18}O is given by Lachniet (2009). One of the main processes acting on both precipitation δ^{18}O and calcite δ^{18}O is temperature. Temperature fractionation on vapor condensation was estimated to be around 0.6‰ °C^{-1} (Rozanski et al., 1992) and the temperature dependent fractionation between cave drip water and speleothem calcite for Han-sur-Lesse Cave was calculated to be -0.2‰ °C^{-1} (Van Rampelbergh et al., 2014). The eventual relation between temperature and speleothem δ^{18}O will be positive, lower temperatures will thus lead to more negative speleothem δ^{18}O. The temperature control has been attributed as one of the main drivers of δ^{18}O fluctuations in European speleothems (Boch et al., 2011, Wainer et al., 2013). In Han-9, this temperature control is well expressed in growth phase 2, where more positive δ^{13}C values, which reflect lower temperatures through changes in vegetation, correspond with more negative δ^{18}O (Fig. 5). This also explains the negative covariation as shown by the Pearson's correlation coefficient for growth phase 2 (Table 2). It is very likely that in this record also the amount of precipitation partly influences the δ^{18}O signal of the speleothem. In the tropics, variations in monsoonal strength are regarded as the main control on speleothem δ^{18}O via the amount effect (Wang et al., 2001) and changes in the amount of precipitation over time have also been considered as a driver for variations within European speleothem δ^{18}O records (Genty et al., 2003; Couchoud et al., 2009, McDermott et al., 2011). Temperature and precipitation (through the amount effect) controls are thus expected to contribute most to the speleothem δ^{18}O variability but as this record covers an interglacial-glacial transition, other processes acting on longer timescales (i.e., fluctuations in global ice-volume) should also be considered. A significant contribution is to be expected from the variations in δ^{18}O of the source, i.e. the North Atlantic Ocean, because of

fluctuations in global ice volume. Waelbroeck et al. (2002) estimated that during MIS 5d, average global δ^{18}O values of ocean waters were up to 0.5‰ higher compared to MIS 5e.

5.3 Climate in the Belgian area between 125.3 and ~97 ka

5.3.1 125.3 ka: Start of speleothem growth triggered by an increase in moisture availability

The age model implies that Han-9 started growing at 125.3 ka (Fig. 4). Among the recent sampling missions for Belgian LIG speleothems, this is the oldest LIG sample found so far (S. Verheyden, pers. comm.). Although a flowstone from the same Han-sur-Lesse Cave was reported to start growing at 130 +/- 10 ka (Quinif and Bastin, 1994), the accuracy of that one single alphaspectrometic dating result can be questioned. Cave systems in Belgium are known to be very sensitive recorders of glacial/interglacial changes, with speleothem deposition only during interglacial intervals (Quinif, 2006). Between 131.5 and 126.5 ka, the Greenland ice sheet experienced enhanced deglacial melting and also reinforced AMOC conditions were present, as identified from the MD04-2845 core from the Bay of Biscay (Sánchez Goñi et al., 2012). Speleothem formation, however, did occur in the Alps and in southern Europe before 125.3 ka (Moseley et al., 2015; Drysdale et al., 2009). This raises the question whether or not the start of Han-9 growth is just sample specific or if it represents a real, although maybe locally confined, climate event at 125.3ka. The SCH-5 alpine speleothem (Fig. 1A) was continuously deposited between 134.1 ± 0.7 and 115.3 ± 0.6 ka (Moseley et al., 2015). Within this record, an increase in the δ^{18}O proxy starting at 128.4 ka and lasting to 125.3 ka was identified as a warming phase. The warming phase recognized in this alpine speleothem occurs just prior to the start of the Han-9 speleothem growth, emphasizing a possible link between the warming and the start of speleothem formation in Han-sur-Lesse. In the BDInf speleothem from southern France (Couchoud et al., 2009) (Fig. 1A), the interval between 125.3 and 123.8 ka was identified as a period with increased rainfall amount. A warmer/wetter period is potentially expressed in northwest European vegetation records as well, such as the Eifel maar record (Sirocko et al., 2005), located only 150km from the cave site in this study. At 125 ka, a transition of a pollen assembly consisting mainly of pioneering *Betula* pollen with boreal *Pinus* towards an assembly significantly richer in thermophilous, broad-leaf tree pollen such as *Ulmus*, *Quercus*, *Corylus* and *Carpinus* is observed. However, the chronology of this record was not constructed independently; the start of the Eemian was determined by cross-correlating with the U/Th dates of the SPA-50 alpine speleothem record of Holzkämper et al. (2004) and set at 127 ka. The Han-9 δ^{13}C record at 125.3 ka has the most negative values for the entire 125.3-117.3 ka growth period, reaching almost -9‰. δ^{18}O on the other hand registers a decrease >0.5‰ during the first 300 years of growth (Fig. 5). The low δ^{13}C values perhaps demonstrate that interglacial optimum conditions were already present before 125.3 ka, but that an increase in moisture availability caused by enhanced precipitation above the cave, shown by the δ^{18}O decrease, was the factor needed to trigger growth of Han-9.

5.3.2 125-120 ka: Eemian optimum

The isotope records of Han-9 are relatively stable between 125 and ~120 ka (Fig. 5). The variation of δ^{18}O seems to be sub-millennial and is largely confined to between -5.7 and -6.3‰. The long-term trend, as displayed by a fitted 7-point running average (Fig. 5), shows lower variability between 125 and ~120 ka, especially when compared to younger growth periods of Han-9 (i.e. 120-117.3 ka and 112.9-106.6 ka). Similar observations are made for δ^{13}C: sub-millennial variability restricted between -7 and -8‰, with the exception of a positive excursion towards -6‰ around 122 ka, and generally more stable than in younger time intervals. During 125-120 ka, other paleoclimate records display stable interglacial conditions, such as speleothems from the Alps

(Meyer et al., 2008; Moseley et al., 2015) and from Italy (Drysdale et al., 2009), and other archives including ice cores (NEEM community, 2013) (Fig. 5). In marine records off the Iberian Margin, the 125-119 ka period was

360   identified as an interval of 'sustained European warmth', following a time of enhanced Greenland melting between 131.5 and 126.5 ka (Sánchez Goñi et al., 2012). We therefore attribute the stability of our records to the Eemian climate optimum persisting in the Belgian area as well. This is also supported by the constant growth rate (Fig. 4) and the speleothem morphology, displaying a sequence of layered calcite which does not show any significant change over the 125-120 ka period (Fig. 2C-E).

365   **5.3.3 120-117.3 ka: Inception of glacial conditions**

At 120 ka, an increase in $\delta^{18}O$ of 0.5‰ is observed (Fig. 5). This change in $\delta^{18}O$ of the speleothem corresponds with an elevated growth rate (Fig. 4) and a speleothem morphology that becomes progressively coarser, with layers that are less expressed (Fig. 2C and E). No major changes in the $\delta^{13}C$ are observed. Although both the age-depth model and the speleothem morphology support an increase in speleothem growth rate, possibly in

370   response to an increase in moisture availability within the cave, there is no evidence in the Han-9 $\delta^{18}O$ record for an increase in precipitation. Due to the amount effect, enhanced precipitation would cause the $\delta^{18}O$ signal to shift towards more negative values, which is not observed in the record. The increase in growth rate and thereby accompanied faster CO_2 degassing during speleothem formation is known to act as a possible kinetic control on the speleothem $\delta^{18}O$ (Hendy, 1971; Lachniet, 2009), yet kinetic control by fast degassing would also result in

375   positive changes of $\delta^{13}C$ (Baker et al., 1997), which is not the case here. Another possible explanation could be a temperature rise causing the elevated $\delta^{18}O$ signal, although such locally confined temperature increase seems unlikely, because no other records (pollen, sea surface temperature) support this hypothesis. Most likely, this increase in $\delta^{18}O$ is not related to any local climate effects but reflects a more regional signal, which could be the increase of the source $\delta^{18}O$ of the North Atlantic Ocean, since a rise of 0.5‰ is in good agreement with

380   estimations of the source $\delta^{18}O$ variability over the MIS 5e/5d transition from Waelbroeck et al. (2002). As a matter of fact, a study by Hearty et al. (2007) combining last interglacial sea-level evolution at 15 sites around the world shows a rapid descent towards an MIS 5d low stand at 119 ± 2 ka. This also favors the hypothesis that the speleothem $\delta^{18}O$ between 120 and 117.3 ka reflects changing ocean source due to ice build-up.

A severe change in the $\delta^{13}C$ is not observed until 117.5 ka, where a sudden increase towards -4‰ occurs (Fig. 5).

385   This 5‰ change takes place within 200 years and happens just before the first hiatus in this speleothem, suggesting that the cessation in speleothem growth is indeed caused by a climate event. The increase in $\delta^{13}C$ here is believed to reflect changes in vegetation, such as an increase grasses resulting in lower vegetation activity, linked to a changing (drying and/or cooling) climate. The age of this event, 117.3 ka, stands out in other studies as well. First of all, in the NGRIP $\delta^{18}O$ record it falls within what is identified as Greenland Stadial 26 (NGRIP

390   Members, 2004). Although the signature of this GS may not be as clear as the younger GS 25 or 24, it corresponds with the overall decreasing trend observed in the ice $\delta^{18}O$, and is also recognized in the more recent NEEM ice core (NEEM community, 2013). The global character of this climate event around 117.3 ka is evidenced by similar changes in the North Atlantic Ocean. A high-resolution study by Galaasen et al. (2014) has found perturbations of the $\delta^{13}C$ of benthic foraminifera in marine sediment cores, interpreted as a sharp decrease

395   in North Atlantic Deep Water (NADW) formation at 116.8 ka, in contrast with the high NADW formation observed during the MIS 5e. Such reductions in NADW led to changes in AMOC, resulting in a reduced ocean heat transport and eventually cooling of the climate. This hypothesis is further evidenced by lower sea surface temperatures, shown by an increase in planktonic foram $\delta^{18}O$, in marine core MD03-2664 at that time (Irvali et

al., 2012) (Fig. 5). The lower resolution in the sea surface temperature record of core MD04-2548 retrieved from the Bay of Biscay (Fig. 1A) could explain its absence in this archive (Fig. 5). Other accurately dated European speleothem records mark a similar climate deterioration around the same time. Perhaps the most obvious example is the study from Meyer et al. (2008), where a 3 to 4‰ drop in $\delta^{18}O$ of four different flowstones from the Entrische Kirche cave (Fig. 1A) is observed between 119 and 118 ka (Fig. 5). This large drop in speleothem $\delta^{18}O$ is believed to be caused by a severe cooling, and was defined as the glacial inception at the cave site. Furthermore, a subtle depletion occurs in the HÖL-10 stalagmite (Fig. 5) and was correlated to the $\delta^{18}O$ drop from Entrische Kirche (Moseley et al., 2015). Closer to the Han-sur-Lesse Cave, a similar event was also observed in the Eifel maar record. There it was identified as the 'LEAP' or the Late Eemian Aridity Pulse and defined by an increase in varve thickness, loess and charcoal content together with a higher abundance of grass pollen within the assembly (Sirocko et al., 2005), which would explain the increase in $\delta^{13}C$ of Han-9. Yet, the timing of the LEAP predates the Han-9 event by ~1 ka. Nevertheless, we suggest that both records registered the same event and that the offset in chronology can be caused by the tuning of the Eifel record or the uncertainty of the Han-9 age-depth model at 117.3ka.

5.3.4 117.3-97 ka: stadial/interstadial changes in the early Weichselian

After the first hiatus, growth starts again at 112.9 ka. The LEAP event in the Eifel maar only lasts 468 years (Sirocko et al., 2005), yet speleothem growth does not recover immediately after the LEAP event. A similar observation was made for the start of speleothem growth at 125.3 ka: optimum conditions were already present before Han-9 started growing. From this delayed growth, it appears that climate conditions need to be more favorable (warmer/wetter) to initiate growth than to sustain growth. During the second growth phase of the Han-9 stalagmite (112.9-106.6 ka), interesting differences occur compared to the earlier formed part of the speleothem. First of all, the variation of both $\delta^{18}O$ and $\delta^{13}C$ is much larger (Fig. 5). Secondly, changes in stalagmite morphology appear, with alternations between dense, darker calcite and more white, coarser calcite (Fig. 2C-E). The $\delta^{13}C$ curve of Han-9 shows a long-term increasing trend until a maximum of -4‰ is reached at 110 ka. Superimposed on this trend, (sub-)millennial variability ranging between 2 and 3‰ is present. In contrast, within the $\delta^{18}O$ record a long-term trend is not as obvious, although a minimum of -6.8‰ is reached between 111 and 110 ka. The maximum in $\delta^{13}C$ and the minimum in $\delta^{18}O$ correspond well with the timing of GS 25 (110.6-108.3 ka, Rasmussen et al., 2014) observed in the NGRIP record (plotted on the GICC05modelext timescale), implying that the stable isotopes of Han-9 reflect the temperature decrease of the stadial, which is likely since higher $\delta^{13}C$ is linked to a less active vegetation cover during colder periods (i.e. more grasses) and lower $\delta^{18}O$ is caused by lower temperatures. The timing in the Han-9 record is also in agreement with the GS 25 registered in the NALPS record, which is believed to be dominantly temperature dependent (Boch et al., 2011). The summer sea surface temperature reconstructions for marine core MD04-2845 show a distinct decrease of ~10°C at the same time (Sánchez Goñi et al., 2012). Between 112.9 and 111 ka, the variability of $\delta^{13}C$ and $\delta^{18}O$ in Han-9, predating GS 25, has an inverse relationship suggesting that $\delta^{18}O$ is mainly temperature controlled. The ice build-up effect, displayed by the increase in $\delta^{18}O$ between 120 and 117.3 ka, is cancelled out by the effect of lower temperature, causing a decrease in speleothem $\delta^{18}O$. It also appears that for a general cooler climate state, the amplitude of variability tends to increase as well, compared to a more stable Eemian optimum (125-120 ka). The timing of the second hiatus (106.6-103 ka) is similar to that of the occurrence of GS 24 in the NGRIP record and is also registered in the NALPS dataset from Boch et al. (2011). However, if the hiatus has any affinity with GS 24, this raises the question why speleothem growth stopped during GS 24 and continued during GS 25. A plausible explanation could be that growth never fully recovered from the GS 25, and that less

favorable conditions (cooler/dryer) during the GS 24 interval were sufficient to cease growth. This assumption is grounded by decreased growth rate from 110 ka onwards (Fig. 4). In the Eifel maar core, significant changes in vegetation occur from ~112 ka, with nearly all pollen from broadleaf trees disappearing and the transition towards a pollen assembly dominated by coniferous trees and grasses (Fig. 5). Also, the time periods 110-108.5 ka and 106-104.5 ka are characterized by a significant increase in loess composition and varve thickness, indicative for dryer conditions in that area and corresponding with the GS 25 and GS 24 intervals (Sirocko et al., 2005).

6. Conclusions

This study highlights the potential of Belgian speleothem proxies (i.e. growth, morphology and stable isotopes) as recorders of regional and local climate change over the Eemian and early Weichselian in northwestern Europe. The start of speleothem growth occurs at 125.3 ka. At that time however, nearly all of the European continental records are already within the Eemian climate optimum state. The δ^{18}O record suggests that the eventual trigger starting speleothem growth was most likely moisture availability, linked to an increase in (local) precipitation at that time. Optimum Eemian climate conditions recorded in Han-9 occurred between 125.3 and 120 ka, and the stable isotopes and speleothem morphology indicate a relatively stable climate state. The first signs of regional changing climate are observed in the δ^{18}O proxy from 120 ka onwards, and are linked to a changing ocean source δ^{18}O, caused by increasing ice volume. The end of the Eemian (and start of the early Weichselian) in Han-9, at 117.3 ka, is preceded by a drastic change in vegetation activity and/or assembly that took place within 200 years, triggered by a decrease in moisture availability linked to a drying climate. This eventually led to cessation of speleothem growth. This event appears to have a broad regional signature, as it is registered in other European records as well. However, pollen records imply that temperate vegetation seems to persist several millennia after 117.3 ka (de Beaulieu and Reille, 1992; Sirocko et al., 2005), resulting in a longer duration of the Eemian in other records (Tzedakis et al., 2003). In addition, Han-9 also registered three stadials occurring during the early Weichselian. During GS 26, at 117.3 ka, the end of the Eemian in Han-9 occurs. The GS 25 equivalent occurs between 110.5 and 108.5 ka as deduced from the stable isotope proxies and GS 24 is represented by a hiatus in Han-9 that starts at 106.6 ka. These chronologies are consistent with other European speleothem records. For the early Weichselian, local climate appears to be more sensitive during the early glacial conditions as the amplitude and frequency of isotopic shifts tends to increase significant compared to the Eemian.

Data availability. Stable isotope time-series for the first two growth phases are available online at NOAA paleoclimate database.

Acknowledgements. We thank the Domaine des Grottes de Han for allowing us to sample the stalagmite and to carry out other fieldwork. S. Vansteenberge thanks D. Verstraeten for the assistance with the stable isotope measurements. Ph. Claeys thanks the Hercules Foundation for upgrade of the Stable Isotope laboratory at VUB, and the VUB Strategic Research funding.

Table 1

Sample Number	DFT (mm)	^{238}U (ppb)	^{232}Th (ppt)	^{230}Th / ^{232}Th (atomic x10^{-6})	δ^{234}U* (measured)	^{230}Th / ^{238}U (activity)	^{230}Th Age (yr) (uncorrected)	^{230}Th Age (yr) (corrected)	δ^{234}U$_{Initial}$** (corrected)	^{230}Th Age (yr BP)*** (corrected)
DAT-10	668	531,5 ±0,6	1693 ±34	6077 ±122	622,5 ±1,5	1,1739 ±0,0016	124854 ±363	124805 ±364	885 ±2	124740 ±364
DAT-1	639	475,3 ±0,4	6419 ±128	1417 ±29	606 ±3	1,1608 ±0,0027	124781 ±653	124569 ±669	862 ±4	124506 ±669
DAT-11	614,6	227,6 ±0,2	413 ±8	11096 ±223	704,0 ±1,6	1,2220 ±0,0013	122075 ±304	122049 ±305	993 ±2	121984 ±305
DAT-12	581,5	289,7 ±0,2	1597 ±32	3563 ±71	675,2 ±1,5	1,1911 ±0,0014	120625 ±304	120542 ±310	949 ±2	120477 ±310
DAT-2	554	370,5 ±0,3	213 ±4	33652 ±692	661 ±3	1,1759 ±0,0029	119934 ±589	119925 ±589	927 ±4	119862 ±589
DAT-13	484,2	390,1 ±0,4	1420 ±28	5246 ±105	637,7 ±1,6	1,1583 ±0,0015	119971 ±331	119915 ±333	895 ±2	119850 ±333
DAT-14	426	337,7 ±0,3	243 ±5	26740 ±539	656,3 ±1,5	1,1679 ±0,0013	119179 ±289	119168 ±289	919 ±2	119103 ±289
DAT-3	397	373,4 ±0,3	681 ±14	10480 ±211	650 ±2	1,1596 ±0,0027	118564 ±539	118536 ±539	908 ±3	118473 ±539
DAT-15	356	636,0 ±0,7	1406 ±28	8600 ±172	648,9 ±1,5	1,1533 ±0,0014	117661 ±306	117627 ±307	904 ±2	117562 ±307
DAT-4	311	226,6 ±0,3	1735 ±35	2526 ±51	667 ±3	1,1727 ±0,0036	118596 ±727	118481 ±731	932 ±5	118418 ±731
DAT-5	297	396,8 ±0,4	563 ±11	13324 ±269	677 ±2	1,1456 ±0,0027	112964 ±512	112942 ±512	931 ±4	112879 ±512
DAT-17	271	213,5 ±0,1	1647 ±33	2460 ±49	692,3 ±1,4	1,1511 ±0,0011	112045 ±237	111930 ±251	949 ±2	111865 ±251
DAT-18	238,5	239,0 ±0,2	208 ±4	21967 ±446	709,8 ±1,6	1,1594 ±0,0012	111337 ±254	111324 ±254	972 ±2	111259 ±254
DAT-6	214	216,2 ±0,3	939 ±19	4315 ±87	691 ±3	1,1365 ±0,0035	109887 ±637	109822 ±638	943 ±4	109759 ±638
DAT-16	201	158,8 ±0,1	386 ±8	7695 ±155	680,1 ±1,5	1,1334 ±0,0012	110663 ±245	110627 ±246	929 ±2	110562 ±246
DAT-19	179,5	179,8 ±0,1	3158 ±63	1064 ±21	711,7 ±1,5	1,1341 ±0,0011	107303 ±223	107042 ±289	963 ±2	106977 ±289
DAT-7	171	187,0 ±0,2	1051 ±21	3255 ±66	712 ±4	1,1089 ±0,0037	103615 ±671	103531 ±673	953 ±6	103468 ±673
DAT-20	154	204,3 ±0,2	2749 ±55	1339 ±27	727,0 ±1,5	1,0929 ±0,0011	99868 ±215	99668 ±257	963 ±2	99603 ±257
DAT-21	125,7	159,7 ±0,1	1709 ±34	1673 ±34	744,0 ±1,6	1,0861 ±0,0011	97373 ±206	97215 ±234	979 ±2	97150 ±234
DAT-8	98,7	149,3 ±0,2	759 ±15	3593 ±73	737 ±4	1,1070 ±0,0039	100847 ±664	100772 ±666	980 ±6	100709 ±666
DAT-22	56	196,9 ±0,1	978 ±20	3503 ±70	694,6 ±1,5	1,0554 ±0,0011	97680 ±206	97604 ±212	915 ±2	97539 ±212
DAT-23	34	234,0 ±0,2	359 ±7	11228 ±226	668,5 ±1,6	1,0444 ±0,0013	98598 ±236	98574 ±237	883 ±2	98509 ±237
DAT-9	15,2	240,4 ±0,2	531 ±11	7898 ±161	677 ±3	1,0581 ±0,0039	99784 ±634	99750 ±634	897 ±4	99687 ±634

U decay constants: λ_{238} = 1.55125x10^{-10} (Jaffey et al., 1971) and λ_{234} = 2.82206x10^{-6} (Cheng et al., 2013). Th decay constant: λ_{230} = 9.1705x10^{-6} (Cheng et al., 2013).

*δ^{234}U = ([^{234}U/^{238}U]$_{activity}$ − 1)x1000. ** δ^{234}U$_{initial}$ was calculated based on ^{230}Th age (T), i.e., δ^{234}U$_{initial}$ = δ^{234}U$_{measured}$ x e$^{\lambda_{234}xT}$.

Corrected ^{230}Th ages assume the initial ^{230}Th/^{232}Th atomic ratio of 4.4 ±2.2 x10^{-6}. Those are the values for a material at secular equilibrium, with the bulk earth ^{232}Th/^{238}U value of 3.8. The errors are arbitrarily assumed to be 50%.

***B.P. stands for "Before Present" where the "Present" is defined as the year 1950 A.D.

Table 1. U/Th measurements of the Han-9 Stalagmite (University of Minnesota). Samples are arranged in stratigraphic order and those in bold indicate results acquired in 2013.

480   **Table 2**

	ρ	# measurements
Growth Phase 1	0,024	599
Growth Phase 2	-0,467	235
Growth Phase 3	0,461	284
Total	-0,197	1118

Table 1: Pearson's coefficient of correlation (ρ) calculated for the three growth phases and for the total record.

	δ^{13}C	δ^{18}O
RC1	-8,19	-5,73
RC2	-8,20	-6,25
RC3	-7,80	-6,48

Table 2: δ^{13}C and δ^{18}O analysis of three recent calcite samples (RC1 to RC3) from the *Réseau Renversé*.

Figure 1

Figure 1 A) Location of the Han-sur-Lesse Cave site (Red Star) and other records mentioned in this study 1) Han-sur-Lesse; 2) Bourgeois-Delaunay Cave (Couchoud et al., 2009); 3) Hölloch Cave (Moseley et al., 2015); 4) Spannagel Cave (Hölzkamper et al., 2004); 5) Entrische Kirche Cave (Meyer et al., 2008); 6) Corchia Cave (Drysdale et al., 2009); 7) MD04-2548 (Sanchez-Goñi et al., 2012); 8) La Grande Pile (Woillard, 1978); 9) Eifel Maar (Sirocko et al., 2005); 10) NGRIP (NGRIP Members, 2004); 11) NEEM (NEEM community, 2013) and 12) MD03-2664 (Irvali et al., 2012). **B)** Topographic map of the study area (source: NGI Belgium). The Han-sur-Lesse Cave system is plotted in black. The sampling site of Han-9 is marked by the yellow dot, the purple dot represents the location of cave monitoring by Van Rampelbergh et al. (2014). The *Réseau Sud* and the *Réseau Renversé* are shown by the red and orange box. For further explanation, see text. Figure adapted from Quinif (2006).
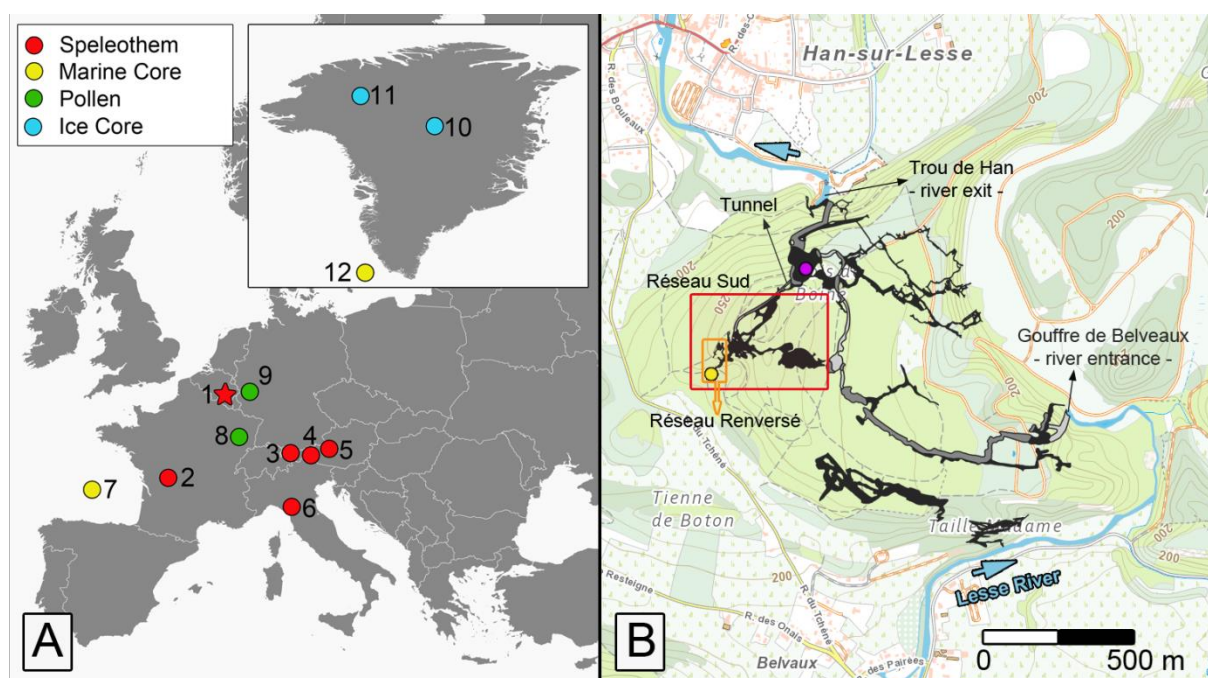
495
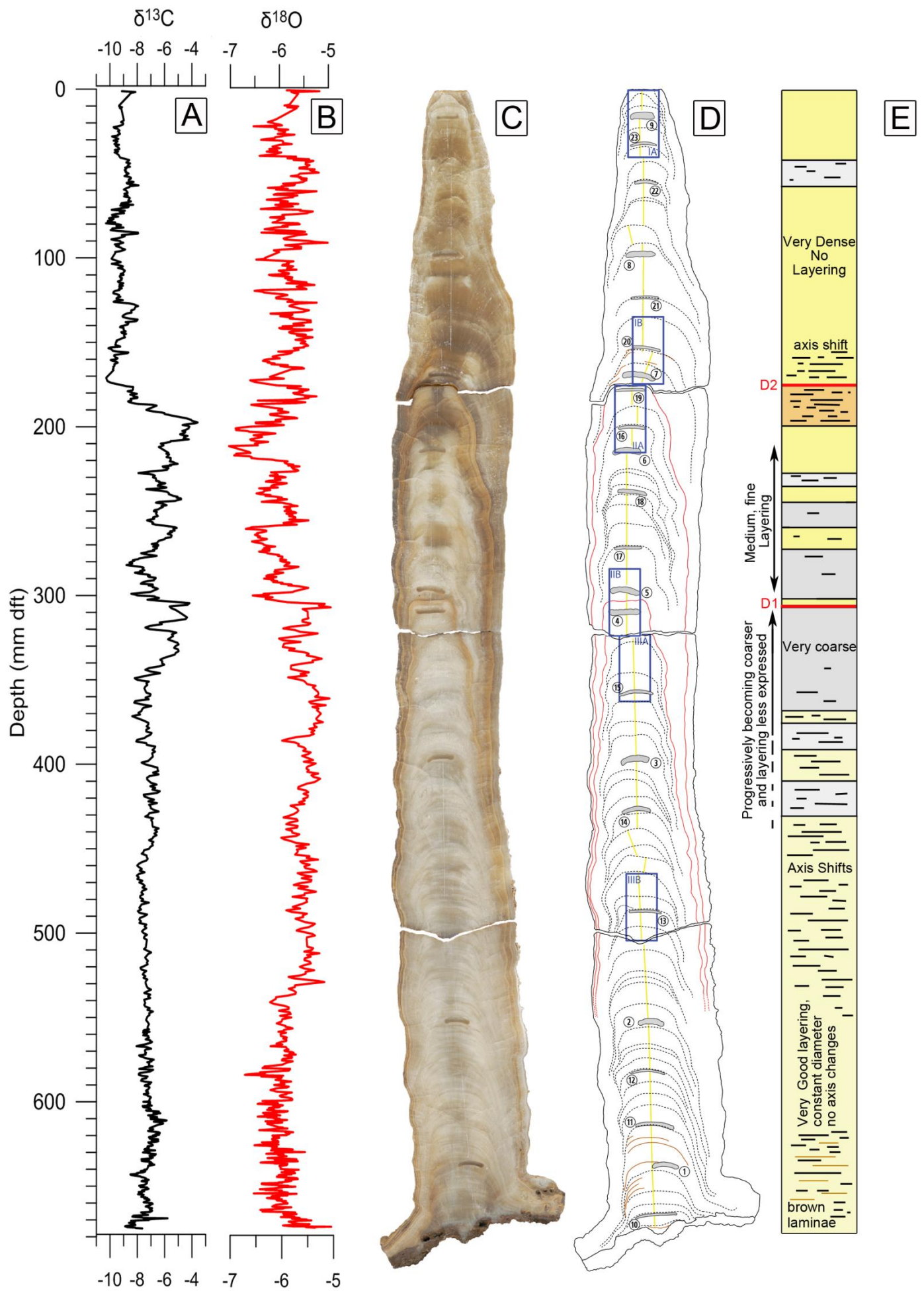
500

Figure 2: Descriptive image of Han-9 **A)** $\delta^{13}C$ plotted against distance from top in mm; **B)** $\delta^{18}O$ plotted against distance from top in mm; **C)** High-resolution scan of the polished slabs; **D)** Interpretation of the internal structure of the speleothem. Dashed lines = distinctive layers; Red lines = growth discontinuities; Grey areas = dating samples, numbers refer to the samples in Table 1; Yellow line = central axis (sample axis); Blue boxes = thin section locations; Brown lines = detrital material. **E)** Stratigraphic log: colors indicate the presence of dense calcite (yellow) or coarse calcite (grey), more intense color = denser/coarser compared to lighter colored parts. The visual expression of layering is indicated with the dashes in the log. Further description of the log can be found in the figure and text.

505

510

Figure 3
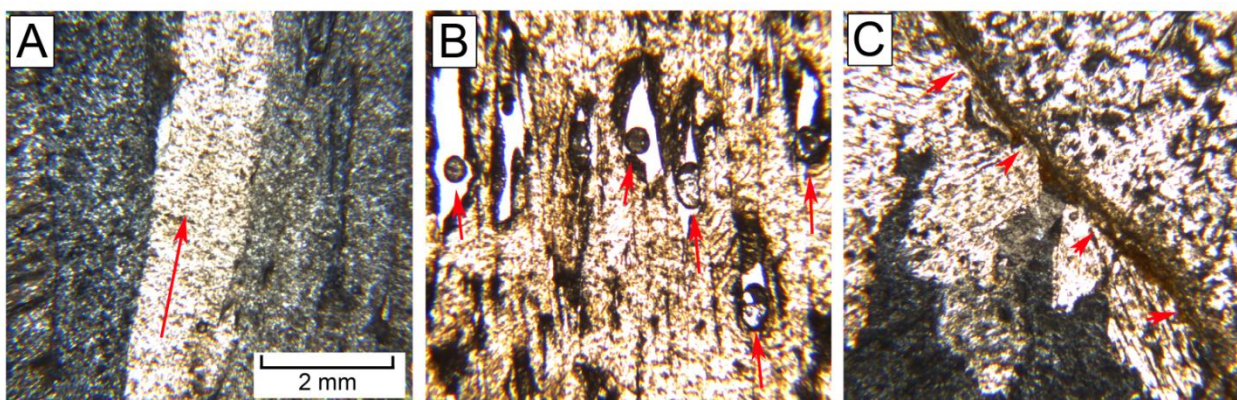
515

Figure 3: Thin section images of the Han-9. For locations, see Fig. 2D. All pictures are taken with crossed polarized light, have the same scale and speleothem growth direction is upwards **A)** Thin section IIIB: (Elongated) columnar calcite fabric. **B)** IIIA: Open columnar fabric, with fluid inclusions in the open voids **C)** IIA: Discontinuity D2 is characterized by presence of brown detrital material. Also note the different fabric underneath the hiatus.

520

525

Figure 4
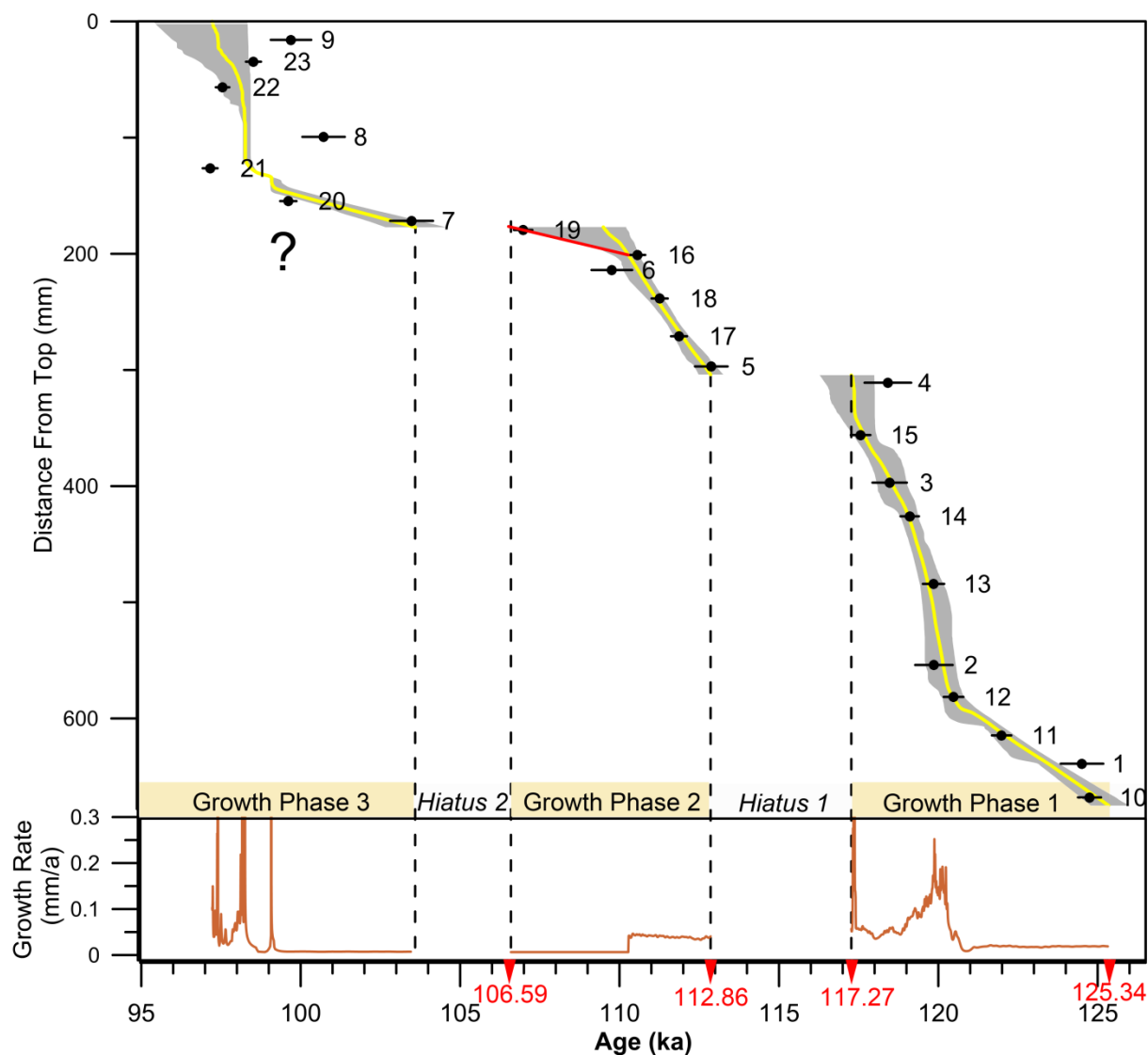
Figure 4: Han-9 age-depth model constructed with the StalAge algorithm (Scholz and Hoffmann, 2011). The actual age-depth model is represented by the yellow line, the grey area marks the error (2σ). Numbers represent the sample labels (Table 1 in original manuscript). The brown curve displays the growth rate. Numbers in red indicate important dates and are discussed in the text.

530

535
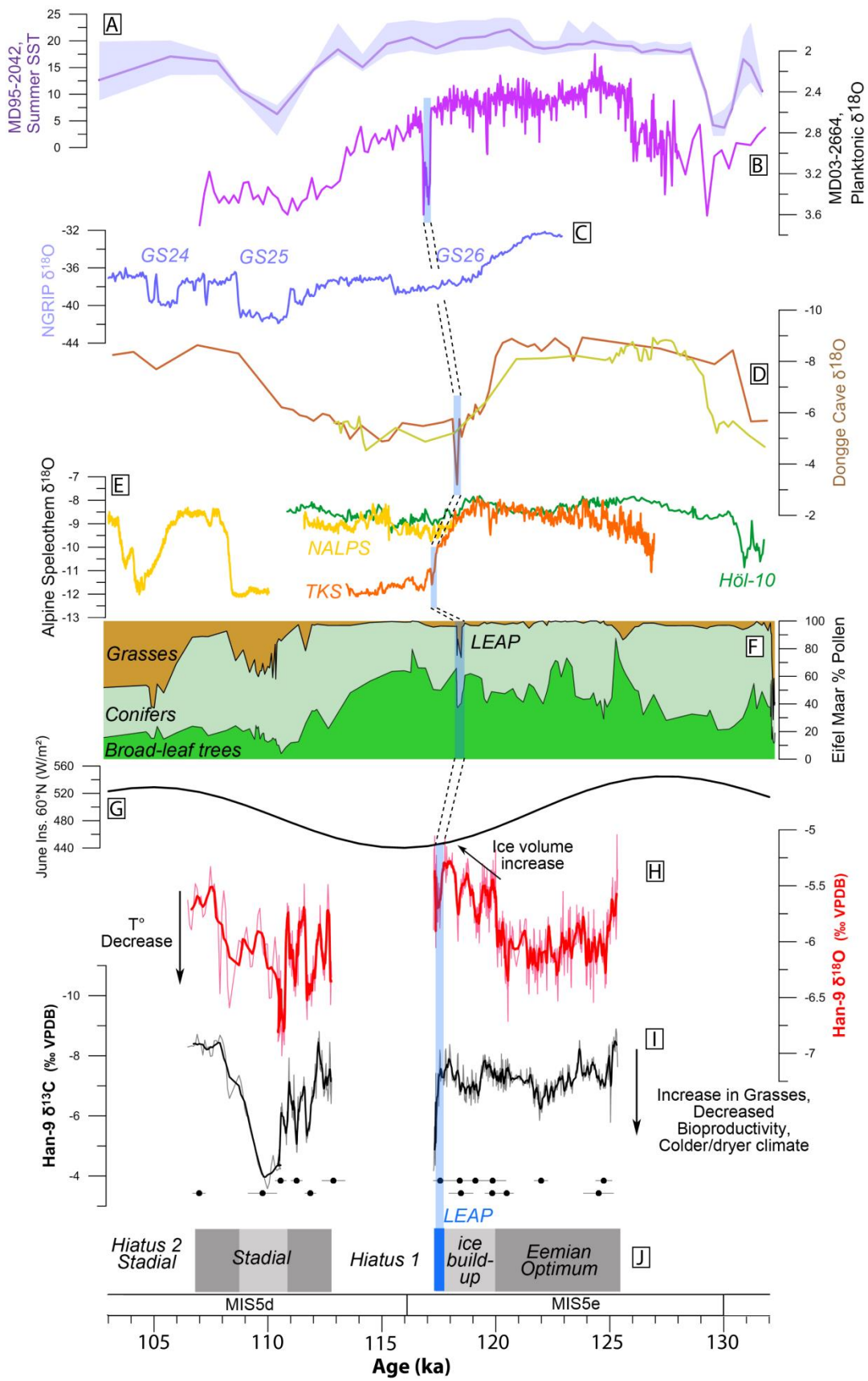
Figure 5

Figure 5: Comparison of Han-9 stalagmite with other records. The shaded blue area marks the occurrence of the Late Eemian Aridity Pulse (LEAP) in the Eifel record and its equivalent in other records. **A)** Sea Surface Temperature (SST) reconstruction from marine core MD04-2845 (Sanchez-Goñi et al., 2012); **B)** Planktonic δ^{18}O from marine core MD03-2664 (Irvali et al., 2012); **C)** NGRIP δ^{18}O record with indication of Greenland Stadial intervals (NGRIP members, 2004); **D)** Asian monsoon reconstructions from Dongge Cave (D3 & D4 stalagmites; Yuan et al., 2004); **E)** Alpine speleothem δ^{18}O (TKS: Meyer et al., 2008; NALPS: Boch et al., 2011; HöL-10: Moseley et al., 2015)**; F)** Eifel Maar pollen assembly (Sirocko et al., 2005); **G)** June insolation for 60°N (Berger and Loutre, 1991); **H)** & **I)** Han-9 stable isotope record with a 7-point moving average and U/Th dates; **J)** Paleoclimate interpretation of Han-9.

References

Baker, A., Ito, E., Smart, P. L., and McEwan, R. F.: Elevated and variable values of C-13 in speleothems in a British cave system, Chemical Geology, 136, 263-270, 10.1016/s0009-2541(96)00129-5, 1997.

Bar-Matthews, M., Ayalon, A., Kaufman, A., and Wasserburg, G. J.: The Eastern Mediterranean paleoclimate as a reflection of regional events: Soreq cave, Israel, Earth and Planetary Science Letters, 166, 85-95, http://dx.doi.org/10.1016/S0012-821X(98)00275-1, 1999.

Barker, S., Chen, J., Gong, X., Jonkers, L., Knorr, G., and Thornalley, D.: Icebergs not the trigger for North Atlantic cold events, Nature, 520, 333-336, 2015.

Bastin, B., and Gewelt, M.: Analyse pollinique et datation 14C de concrétions stalagmitiques Holocènes: apportes complémentaires des deux méthodes, Géographie physique et Quaternaire, 40, 185-196, 1986.

Berger, A., and Loutre, M. F.: An Exceptionally Long Interglacial Ahead?, Science, 297, 1287-1288, 10.1126/science.1076120, 2002.

Boch, R., Cheng, H., Spotl, C., Edwards, R. L., Wang, X., and Hauselmann, P.: NALPS: a precisely dated European climate record 120-60 ka, Climate of the Past, 7, 1247-1259, 10.5194/cp-7-1247-2011, 2011.

Bond, G., Broecker, W., Johnsen, S., McManus, J., Labeyrie, L., Jouzel, J., and Bonani, G.: Correlations between climate records from North-Atlantic sediments and Greenlan Ice, Nature, 365, 143-147, 10.1038/365143a0, 1993.

Bond, G. C.: Climate and the conveyor, Nature, 377, 383-384, 1995.

Bonniver, I.: Hydrogéologie du Massif de Boine, in: EcoKarst, 3, La Hulpe, 1-4, 2010.

Bonniver, I.: Etude Hyrogeologique et dimmensionnement par modelisation du "systeme-tracage" du reseau karstique the Han-sur-Lesse (Massif de Boine, Belgique), in: Géologie, FUNDP Namur, Namur, 93-97, 2011.

Broecker, W. S., Peteet, D. M., and Rind, D.: Does the ocean-atmosphere system have more than one stable mode of operation?, Nature, 315, 21-26, 1985.

Couchoud, I., Genty, D., Hoffmann, D., Drysdale, R., and Blamart, D.: Millennial-scale climate variability during the Last Interglacial recorded in a speleothem from south-western France, Quaternary Science Reviews, 28, 3263-3274, 10.1016/j.quascirev.2009.08.014, 2009.

Cheng, H., Edwards, R. L., Chuan-Chou, S., Polyak, V. J., Asmerom, Y., Woodhead, J., Hellstrom, J., Yongjin, W., Xinggong, K., Spotl, C., Xianfeng, W., and Alexander, E. C., Jr.: Improvements in 230Th dating, 230Th and 234U half-life values, and U-Th isotopic measurements by multi-collector inductively coupled plasma mass spectrometry, Earth and Planetary Science Letters, 371-372, 82-91, 10.1016/j.epsl.2013.04.006, 2013.

Dansgaard, W., Johnsen, S. J., Clausen, H. B., Dahl-Jensen, D., Gundestrup, N. S., Hammer, C. U., Hvidberg, C. S., Steffensen, J. P., Sveinbjornsdottir, A. E., Jouzel, J., and Bond, G.: Evidence for general instability of past climate from a 250-kyr ice-core record, Nature, 364, 218-220, 1993.

de Beaulieu, J.-L.: Pollen Profile GPILXX, La Grande Pile, France, edited by: de Beaulieu, J.-L., Pangaea,

European Pollen Database, 2010.

de Beaulieu, J. L., and Reille, M.: The last climatic cycle at La Grande Pile (Vosges, France) a new pollen
580   profile, Quaternary Science Reviews, 11, 431-438, http://dx.doi.org/10.1016/0277-3791(92)90025-4, 1992.

Dorale, J. A., Liu, Z.: Limitations of Hendy test criteria in judging the paleoclimatic suitability of speleothems
and the need for replication, Journal of Cave and Karst Studies, 71, 73-80, 2009.

Drysdale, R. N., Zanchetta, G., Hellstrom, J. C., Fallick, A. E., McDonald, J., and Cartwright, I.: Stalagmite
evidence for the precise timing of North Atlantic cold events during the early last glacial, Geology, 35, 77-80,
585   2007.

Drysdale, R. N., Hellstrom, J. C., Zanchetta, G., Fallick, A. E., Sánchez Goñi, M. F., Couchoud, I., McDonald,
J., Maas, R., Lohmann, G., and Isola, I.: Evidence for Obliquity Forcing of Glacial Termination II, Science, 325,
1527-1531, 2009.

Dutton, A., and Lambeck, K.: Ice Volume and Sea Level During the Last Interglacial, Science, 337, 216-219,
590   10.1126/science.1205749, 2012.

Edwards, R. L., Chen, J. H., Ku, T. L., and Wasserburg, G. J.: Precise Timing of the Last Interglacial Period
from Mass Spectrometric Determination of Thorium-230 in Corals, Science, 236, 1547-1553, 1987.

Ehleringer, J. E., Cerling, T. E., Helliker, B. R., C4 photoynthesis, atmospheric CO2, and climate, Oecologia,
112, 285-299, 1997.

595   Fairchild, I. J., Smith, C. L., Baker, A., Fuller, L., Spotl, C., Mattey, D., McDermott, F., and Eimp: Modification
and preservation of environmental signals in speleothems, Earth-Science Reviews, 75, 105-153,
10.1016/j.earscirev.2005.08.003, 2006.

Fairchild, I., and Baker, A.: Speleothem Science: from Process to Past Environments, Wiley-Blackwell, 2012.

Friedman, I., O'Neil, J., and Cebula, G.: Two New Carbonate Stable-Isotope Standards, Geostandards
600   Newsletter, 6, 11-12, 10.1111/j.1751-908X.1982.tb00340.x, 1982.

Frisia, S.: Microstratigraphic logging of calcite fabrics in speleothems as tool for palaeoclimate studies,
International Journal of Speleology, 44, 1-16, 10.5038/1827-806x.44.1.1, 2015.

Galaasen, E. V., Ninnemann, U. S., Irvali, N., Kleiven, H. F., Rosenthal, Y., Kissel, C., and Hodell, D. A.: Rapid
Reductions in North Atlantic Deep Water During the Peak of the Last Interglacial Period, Science, 343, 1129-
605   1132, 10.1126/science.1248667, 2014.

Gascoyne, M.: Paleoclimate determination from cave calcite deposits, Quaternary Science Reviews, 11, 609-
632, 10.1016/0277-3791(92)90074-i, 1992.

Genty, D., Blamart, D., Ouahdi, R., Gilmour, M., Baker, A., Jouzel, J., and Van-Exter, S.: Precise dating of
Dansgaard-Oeschger climate oscillations in western Europe from stalagmite data, Nature, 421, 833-837,
610   2003.Genty, D., Verheyden, S., and Wainer, K.: Speleothem records over the Last Interglacial, 1, PAGES, 24-
25, 2013.

Gewelt, M., and Ek, C.: Les Concrétions Carbonatees des Grottes: aperçu synthetique, Annales de la Société
géologique de Belgique, 111, 9-19, 1988.

Gimeno, L., Drumond, A., Nieto, R., Trigo, R. M., Stohl, A.: On the origin of continental precipitation,
615   Geophysical Research Letters, 37, L13804, doi:10.1029/2010GL043712, 2010. Goelzer, H., Huybrechts, P., Loutre,
M. F., and Fichefet, T.: Impact of ice sheet meltwater fluxes on the climate evolution at the onset of the Last
Interglacial, Clim. Past Discuss., 11, 4391-4423, 10.5194/cpd-11-4391-2015, 2015.

Hearty, P. J., Hollin, J. T., Neumann, A. C., O'Leary, M. J., and McCulloch, M.: Global sea-level fluctuations during the Last Interglaciation (MIS 5e), Quaternary Science Reviews, 26, 2090-2112,

620 10.1016/j.quascirev.2007.06.019, 2007.

Helmens, K. F.: The Last Interglacial Glacial cycle (MIS 5-2) re-examined based on long proxy records from central and northern Europe, Quaternary Science Reviews, 86, 115-143, 10.1016/j.quascirev.2013.12.012, 2014.

Hendy, C. H.: Isotopic geochemistry of speleothems. 1. Calculation of effect of different modes of formation on isotopic compositions of speleothems and their applicability as paleoclimatic indicators, Geochimica Et

625 Cosmochimica Acta, 35, 801-824, 10.1016/0016-7037(71)90127-x, 1971.

Holzkamper, S., Mangini, A., Spotl, C., and Mudelsee, M.: Timing and progression of the Last Interglacial derived from a high alpine stalagmite, Geophysical Research Letters, 31, 4, 10.1029/2003gl019112, 2004.

Irvali, N., Ninnemann, U. S., Galaasen, E. V., Rosenthal, Y., Kroon, D., Oppo, D. W., Kleiven, H. F., Darling, K. F., and Kissel, C.: Rapid switches in subpolar North Atlantic hydrography and climate during the Last

630 Interglacial (MIS 5e), Paleoceanography, 27, 16, 10.1029/2011pa002244, 2012.

Kukla, G. J., Bender, M. L., de Beaulieu, J. L., Bond, G., Broecker, W. S., Cleveringa, P., Gavin, J. E., Herbert, T. D., Imbrie, J., Jouzel, J., Keigwin, L. D., Knudsen, K. L., McManus, J. F., Merkt, J., Muhs, D. R., Muller, H., Poore, R. Z., Porter, S. C., Seret, G., Shackleton, N. J., Turner, C., Tzedakis, P. C., and Winograd, I. J.: Last interglacial climates, Quaternary Research, 58, 2-13, 10.1006/qres.2002.2316, 2002.

635 Lachniet, M. S.: Climatic and environmental controls on speleothem oxygen-isotope values, Quaternary Science Reviews, 28, 412-432, 10.1016/j.quascirev.2008.10.021, 2009.

Loutre, M. F., Fichefet, T., Goosse, H., Huybrechts, P., Goelzer, H., and Capron, E.: Factors controlling the last interglacial climate as simulated by LOVECLIM1.3, Clim. Past, 10, 1541-1565, 10.5194/cp-10-1541-2014, 2014.

640 Martinson, D. G., Pisias, N. G., Hays, J. D., Imbrie, J., Moore, T. C., and Shackleton, N. J.: Age dating and the orbital theory of the ice ages: Development of a high-resolution 0 to 300,000-year chronostratigraphy, Quaternary Research, 27, 1-29, http://dx.doi.org/10.1016/0033-5894(87)90046-9, 1987.

McDermott, F.: Palaeo-climate reconstruction from stable isotope variations in speleothems: a review, Quaternary Science Reviews, 23, 901-918, http://dx.doi.org/10.1016/j.quascirev.2003.06.021, 2004.

645 McDermott, F., Atkinson, T. C., Fairchild, I. J., Baldini, L. M., and Mattey, D. P.: A first evaluation of the spatial gradients in delta O-18 recorded by European Holocene speleothems, Global and Planetary Change, 79, 275-287, 10.1016/j.gloplacha.2011.01.005, 2011.

McManus, J. F., Bond, G. C., Broecker, W. S., Johnsen, S., Labeyrie, L., and Higgins, S.: High-resolution climate records from the North Atlantic during the last interglacial, Nature, 371, 326-329, 1994.

650 Meyer, M. C., Spotl, C., and Mangini, A.: The demise of the Last Interglacial recorded in isotopically dated speleothems from the Alps, Quaternary Science Reviews, 27, 476-496, 10.1016/j.quascirev.2007.11.005, 2008.

Moseley, G. E., Spötl, C., Cheng, H., Boch, R., Min, A., and Edwards, R. L.: Termination-II interstadial/stadial climate change recorded in two stalagmites from the north European Alps, Quaternary Science Reviews, 127, 229-239, http://dx.doi.org/10.1016/j.quascirev.2015.07.012, 2015.

655 NEEM community: Eemian interglacial reconstructed from a Greenland folded ice core, Nature, 493, 489-494, 10.1038/nature11789, 2013.

NGRIP members.: High-resolution record of Northern Hemisphere climate extending into the last interglacial period, Nature, 431, 147-151, 2004.

Otto-Bliesner, B. L., Rosenbloom, N., Stone, E. J., McKay, N. P., Lunt, D. J., Brady, E. C., and Overpeck, J. T.:

660 How warm was the last interglacial? New model - data comparisons, Philosophical Transactions of the Royal

Society A: Mathematical, Phys. Engin. Sci., 371, 1–20, 2013.

Otvos, E. G.: The Last Interglacial Stage: Definitions and marine highstand, North America and Eurasia,

Quaternary International, 383, 158-173, http://dx.doi.org/10.1016/j.quaint.2014.05.010, 2015.

Petit, J. R., Jouzel, J., Raynaud, D., Barkov, N. I., Barnola, J. M., Basile, I., Bender, M., Chappellaz, J., Davis,

665 M., Delaygue, G., Delmotte, M., Kotlyakov, V. M., Legrand, M., Lipenkov, V. Y., Lorius, C., Pepin, L., Ritz,

C., Saltzman, E., and Stievenard, M.: Climate and atmospheric history of the past 420,000 years from the Vostok

ice core, Antarctica, Nature, 399, 429-436, 10.1038/20859, 1999.

Pyankov, V. I., Ziegler, H., Akhani, H., Deigele, C., Lüttge, U.: European plants with C4 photosynthesis:

geographical and taxonomic distribution and relations to climate parameters, Botanical Journal of the Linnean

670 Society, 163, 283-304, 2010. Quinif, Y., and Bastin, B.: Datation Uranium/Thorium et Analyse Pollinique d'une

Séquence Stalagmitique du Stade 5 (Galerie des Verviétois, Grotte de Han-sur-Lesse, Belgique), Comptes

Rendus de l'Académie des Sciences, 318, 211-217, 1994.

Quinif, Y.: Complex stratigraphic sequences in Belgian caves: correlation with climate changes during the

Middle, the Upper Pleistocene and the Holocene.   , Geologica Belgica, 9, 231-244, 2006.

675 Rasmussen, S. O., Bigler, M., Blockley, S. P., Blunier, T., Buchardt, S. L., Clausen, H. B., Cvijanovic, I., Dahl-

Jensen, D., Johnsen, S. J., Fischer, H., Gkinis, V., Guillevic, M., Hoek, W. Z., Lowe, J. J., Pedro, J. B., Popp, T.,

Seierstad, I. K., Steffensen, J. P., Svensson, A. M., Vallelonga, P., Vinther, B. M., Walker, M. J. C., Wheatley, J.

J., Winstrup, M.: A stratigraphic framework for abrupt climatic changes during the Last Glacial period based on

three synchronized Greenland ice-core records: refining and extending the INTIMATE event stratigraphy,

680 Quaternary Science Reviews, 106, 14-28, 2014.

Riechelmann, D. F. C., Schroeder-Ritzrau, A., Scholz, D., Fohlmeister, J., Spoetl, C., Richter, D. K., Mangini,

A.: Monitoring Bunker Cave (NW Germany): A prerequisite to interpret geochemical proxy data of speleothems

from this site, Journal of Hydrology, 409, 682-695, 2011.Rozanski, K., Araguasaraguas, L., and Gonfiantini, R.:

Relation between long-term trends of 18-O isotope composition of precipitation and climate, Science, 258, 981-

685 985, 10.1126/science.258.5084.981, 1992.

Sánchez Goñi, M. F., Eynaud, F., Turon, J. L., and Shackleton, N. J.: High resolution palynological record off

the Iberian margin: direct land-sea correlation for the Last Interglacial complex, Earth and Planetary Science

Letters, 171, 123-137, http://dx.doi.org/10.1016/S0012-821X(99)00141-7, 1999.

Sánchez Goñi, M. F., Bakker, P., Desprat, S., Carlson, A. E., Van Meerbeeck, C. J., Peyron, O., Naughton, F.,

690 Fletcher, W. J., Eynaud, F., Rossignol, L., and Renssen, H.: European climate optimum and enhanced Greenland

melt during the Last Interglacial, Geology, 40, 627-630, 10.1130/g32908.1, 2012.

Scholz, D., and Hoffmann, D. L.: StalAge - An algorithm designed for construction of speleothem age models,

Quaternary Geochronology, 6, 369-382, 10.1016/j.quageo.2011.02.002, 2011.

Schubert, B. A., and Jahren, A. H.: The effect of atmospheric CO2 concentration on carbon isotope fractionation

695 in C3 land plants, Geochimica et Cosmochimica Acta, 96, 29-43, http://dx.doi.org/10.1016/j.gca.2012.08.003,

2012.

Shackleton, N. J.: Last Interglacial in marine and terrestrial records, Proceedings of the Royal Society Series B-

Biological Sciences, 174, 135-+, 10.1098/rspb.1969.0085, 1969.

Shen, C. C., Wu, C. C., Cheng, H., Edwards, R. L., Hsieh, Y. T., Gallet, S., Chang, C. C., Li, T. Y., Lam D. D.,

700 Kano, A., Hori, M., Spötl, C.: High-precision and high-resolution carbonate 230Th dating by MC-ICP-MS with

SEM protocols, Geochimica et Cosmochimica Acta, 99, 71-86, 2012.

Sirocko, F., Seelos, K., Schaber, K., Rein, B., Dreher, F., Diehl, M., Lehne, R., Jager, K., Krbetschek, M., and Degering, D.: A late Eemian aridity pulse in central Europe during the last glacial inception, Nature, 436, 833-836, 2005.

705 Soreng, R. J., Peterson, P. M., Romaschenko, K., Davidse, G., Zuloaga, F. O., Judziewicz, E. J., Filguieras, T. S., Davis, J. I., Morrone, O.: A worldwide phylogenetic classification of the Poaceae (Gramineae), Journal of Systematics and Evolution, 53(2), 117-137, 2015.Timperman, M.: La Grotte de Han: Au Fil de Siècles, Gembloux, 66 pp., 1989.

Tzedakis, P. C., Frogley, M. R., and Heaton, T. H. E.: Last Interglacial conditions in southern Europe: evidence

710 from Ioannina, northwest Greece, Global and Planetary Change, 36, 157-170, http://dx.doi.org/10.1016/S0921-8181(02)00182-0, 2003.

van Kreveld, S., Sarnthein, M., Erlenkeuser, H., Grootes, P., Jung, S., Nadeau, M. J., Pflaumann, U., and Voelker, A.: Potential links between surging ice sheets, circulation changes, and the Dansgaard-Oeschger Cycles in the Irminger Sea, 60–18 Kyr, Paleoceanography, 15, 425-442, 10.1029/1999PA000464, 2000.

715 Van Rampelbergh, M., Verheyden, S., Allan, M., Quinif, Y., Keppens, E., and Claeys, P.: Monitoring of a fast-growing speleothem site from the Han-sur-Lesse Cave, Belgium, indicates equilibrium deposition of the seasonal δ18O and δ13C signals in the calcite, Clim. Past, 10, 1871-1885, 10.5194/cp-10-1871-2014, 2014.

Van Rampelbergh, M., Verheyden, S., Allan, M., Quinif, Y., Cheng, H., Edwards, L. R., Keppens, E., and Claeys, P.: A 500-year seasonally resolved δ18O and δ13C, layer thickness and calcite aspect record from a

720 speleothem deposited in the Han-sur-Lesse Cave, Belgium, Clim. Past, 11, 789-802, 10.5194/cp-11-789-2015, 2015.

Verheyden, S., Baele, J. M., Keppens, E., Genty, D., Cattani, O., Hai, C., Edwards, L., Hucai, Z., Van Strijdonck, M., and Quinif, Y.: The proserpine stalagmite (Han-sur-Lesse Cave, Belgium): Preliminary environmental interpretation of the last 1000 years as recorded in a layered speleothem, Geologica Belgica, 9,

725 245-256, 2006.

Verheyden, S., Genty, D., Deflandre, G., Quinif, Y., and Keppens, E.: Monitoring climatological, hydrological and geochemical parameters in the Pere Noel cave (Belgium): implication for the interpretation of speleothem isotopic and geochemical time-series, International Journal of Speleology, 37, 221-234, 2008.

Verheyden, S.: The 8.2 ka event: is it registered in Belgian speleothems?, Speleogenesis and Evolution of Karst

730 Aquifers, 3-8, 2012.

Verheyden, S., Keppens, E., Quinif, Y., Cheng, H. J., and Edwards, L. R.: Late-glacial and Holocene climate reconstruction as inferred from a stalagmite - Grotte du Pere Noel, Han-sur-Lesse, Belgium, Geologica Belgica, 17, 83-89, 2014.

Waelbroeck, C., Labeyrie, L., Michel, E., Duplessy, J. C., McManus, J. F., Lambeck, K., Balbon, E., and

735 Labracherie, M.: Sea-level and deep water temperature changes derived from benthic foraminifera isotopic records, Quaternary Science Reviews, 21, 295-305, 10.1016/s0277-3791(01)00101-9, 2002.

Wainer, K., Genty, D., Blamart, D., Bar-Matthews, M., Quinif, Y., and Plagnes, V.: Millennial climatic instability during penultimate glacial period recorded in a south-western France speleothem, Palaeogeography Palaeoclimatology Palaeoecology, 376, 122-131, 10.1016/j.palaeo.2013.02.026, 2013.

740 Wang, Y. J., Cheng, H., Edwards, R. L., An, Z. S., Wu, J. Y., Shen, C. C., and Dorale, J. A.: A High-Resolution Absolute-Dated Late Pleistocene Monsoon Record from Hulu Cave, China, Science, 294, 2345-2348, 2001.

Wohlfarth, B.: A review of Early Weichselian climate (MIS 5d-a) in Europe, Swedish Nuclear Fuel and Waste Management Co, 2013.

Woillard, G. M.: Grande Pile peat bog: A continuous pollen record for the last 140,000 years, Quaternary

745 Research, 9, 1-21, http://dx.doi.org/10.1016/0033-5894(78)90079-0, 1978.

Wong, C. I., and Breecker, D. O.: Advancements in the use of speleothems as climate archives, Quaternary Science Reviews, 127, 1-18, http://dx.doi.org/10.1016/j.quascirev.2015.07.019, 2015.

Yuan, D., Cheng, H., Edwards, R. L., Dykoski, C. A., Kelly, M. J., Zhang, M., Qing, J., Lin, Y., Wang, Y., Wu, J., Dorale, J., An, Z., Cai, Y.: Timing, Durqtion and Transition of the Last Interglacial Asian Monsoon, Science,

750 304, 575-578, 2004.